Non-linear thermal simulation at system level: Compact modelling and experimental validation

Non-linear Thermal Simulation at System Level: Compact Modelling and Experimental Validation

Mirko Bernardoni*, Nicola Delmonte†, Diego Chiozzi†, Paolo Cova†

* KAI Kompetenzzentrum Automobil- und Industrieelektronik GmbH

†University of Parma, Dipartimento di Ingegneria dell'Informazione

Corresponding author: Dr. Mirko Bernardoni, mirko.bernardoni@k-ai.at, *tel.*: +43 051 777 19933

address: KAI GmbH, Europastrasse 8, 9524, Villach (Austria)

Abstract

In this work, a general methodology to extract compact, non-linear transient thermal models of complex thermal systems is presented and validated. The focus of the work is to show a robust method to develop compact and accurate non-linear thermal models in the general case of systems with multiple heat sources. A real example of such a system is manufactured and its thermal behavior is analyzed by means of Infra-Red thermography measurements. A transient, non-linear Finite-Element-Method based model is therefore built and tuned on the measured thermal responses. From this model, the transient thermal responses of the system are calculated in the locations of interest. From these transient responses, non-linear compact transient thermal models are derived. These models are based on Foster network topology and they can capture the effect of thermal non-linearities present in any real thermal system, accounting for mutual interaction between different power sources. The followed methodology is described, verification of the model against measurements is performed and limitations of the approach are therefore discussed. The developed methodology shows that it is possible to capture strongly non-linear effects in multiple-heat source systems with very good accuracy, enabling fast and accurate thermal simulations in electrical solvers.

Keywords: Modeling, Infrared Measurements, Simulation, Circuit simulation

This work has not been submitted elsewhere.

I. Introduction

Many compact thermal modelling methods, which use RC networks to describe heat propagation for certain boundary conditions, can be found in the literature.

For instance, Szekely has been focusing on infinite RC transmission lines, Network Identification via Deconvolution (NID) [1], [2], the concept of structure function in electronic packages [3]; the work carried out in the framework of the DELPHI project, aimed at the determination of Boundary-Condition-Independent (BCI) compact thermal models of several packages used in electronic industry, see [4], [5]. Schweitzer [6] showed several methods about how to determine the parameters of a thermal network with *a priori* defined topology; Model-Order-Reduction techniques represent an efficient way to reduce model complexity and such an approach can be found in [7].

Lumped Element (LE) models can be discerned in *physical models*, strictly connected to the physical layers and features of the described systems [8], and *empirical models*, which aim at capturing a given response of the studied system [9], [10]. Lumped element physical models tend to be cumbersome to be built, losing their appeal in terms of computational lightness. Therefore, it makes sense to invest effort in developing accurate *behavioral* models. In the field of compact thermal models, a general approach to their determination can be found in [11], while examples of their applications to electro-thermally coupled simulations or coupling with different dynamics can be found in [12] – [17]. An example of how to insert lumped element models in an FEM model is shown in [18].

A general methodology which allows to determine lumped element models should produce accurate, fast, non-linear models; the presence of multiple heat sources should also be considered. Finite Element Method (FEM) is currently the simulation tool which offers most of the required features, at the cost of simulation speed [19], [20]; on the other hand, standard lumped element models offer the best in terms of simulation speed, but they may easily lack in terms of description of non-linearities and accuracy.

In this work, a robust procedure to generate such compact models fullfilling all the above mentioned requirements is described in detail, together with its validation on an *ad-hoc* test structure.

II. Determination of Foster networks

In this section, a method to obtain a non-linear Foster network from a set of thermal impedance curves obtained at different power dissipation levels is shown.

A. Linear Foster networks

The thermal impedance response $Z_{th}(t)$ of a given system is usually described by a series of K exponential terms:

$$Z_F(t) = \sum_{k=1}^{K} R_k(1 - \exp(-t/\tau_k)) \tag{1}$$

with obvious meaning of the symbols. To determine all the parameters, a logarithmically-spaced set of time constants τ_k between two reasonable extremes is generated [21], followed by the minimization of the difference between the measured response $Z_F(t)$ and the calculated one:

$$\min \sum_{t=t_0}^{t=t_s} (Z_F(t) - Z_{th}(t))^2 \tag{2}$$

where $t_0, \ldots, t_s$ are the time instants at which both waveforms are sampled. The fitting parameters in Equation (2) are the number of stages K and each of the R_k resistances. The minimization can be performed iteratively by increasing the number of stages until a satisfactory fit is achieved, with the lowest number of stages K as possible. Such algorithm can be easily implemented in Python [22] by using the NumPy [23] and SciPy [24] modules.

B. Non-linear Foster networks

A non-linear Foster network can be though as a merging of several Foster networks, each of which described like in Equation (1). In case of a non-linear system, different power dissipation levels P_0, P_1 will lead to different responses:

$$Z_{th0}(t) = \frac{\Delta T(t)}{P_0} = \sum_{k=1}^{K_0} R_{k0}(1 - \exp(-t/\tau_{k0})) \tag{3}$$

$$Z_{th1}(t) = \frac{\Delta T(t)}{P_1} = \sum_{k=1}^{K_1} R_{k1}(1 - \exp(-t/\tau_{k1})) \tag{4}$$

with $K_0 \neq K_1$ in general, as well as the R_{k0}, R_{k1} and τ_{k0}, τ_{k1} constants.

It is always possible to find a value $K \geq \max(K_0, K_1)$, for which the two responses are both equally well described, both with the *same number of terms*. Calling Q the number of power dissipation levels, this observation can be easily generalized to $Q > 2$.

Therefore, if the topology of the network is fixed i.e., the amount of stages K needed is the same for every power dissipation level, it is possible to collapse all the linear Foster networks into a *single*, *non-linear* Foster network. The terms $R_1, R_2, \ldots, R_K$ are dependent on the temperature of the network's first node (which is the only node with a physical meaning).

The topology is therefore described in Fig. 1 where only three stages are drawn, for sake of simplicity.

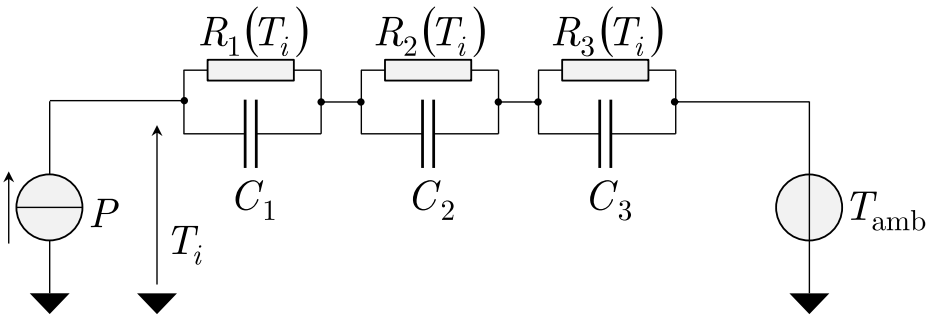

Fig. 1. An exemplary non-linear Foster network with three stages.

Accurate non-linear models can be built only with non-linear resistive terms, keeping the capacitive terms constant [25].

Moreover, numerical problems are reduced if the variation of each of the terms $R_1(T)$, $R_2(T)$, $\ldots$, $R_k(T)$ is monotonic. It was noted that the best number of stages which satisfies the listed requirements was characterized by a (not strictly) monotonic behavior of the non-linear, resistive terms as a function of the input temperature. Should this not be case, it is sufficient to increase the number of stages K.

The procedure to determine the non-linear thermal models here shown consists of the following steps:

1) generate a set of Z_{th} curves for increasing *power dissipation* levels $P_1, \ldots, P_Q$ with $P_1 < P_2 < \cdots < P_Q$;
2) starting from the lowest power level P_q with $q = 1$, perform the standard procedure to

obtain a linear Foster network which describes this very thermal impedance; an initial number of stages K will be obtained;

3) go to the next power level P_{q+1} and perform again the standard procedure to obtain a linear Foster network, using the coefficients obtained at the previous step P_q as starting guess points for the optimization; at the end of this step, q Foster networks, each of which made of K stages, are obtained;
4) check the series of values obtained for $R_1, \ldots, R_K$; if the fitting is consistent for each power level and the monotonicity of each resistive terms is respected, the procedure is successful. Otherwise, repeat from step 2) with $K = K + 1$.

The monotonicity of the resistive terms can be obtained by careful selection of the time constants which are used to perform the fit. By finely increasing the P_q values, the typical time constants will also vary slightly and the monotonicity of the resistive terms can be easily achieved.

Basically, the correct Foster network is the one for which the following equations hold:

$$Z_{th}(t) = \sum_{k=1}^{K} R_k(T)(1 - e^{-t/\tau_k(T)}) \tag{5}$$

$$\frac{dR_k(T)}{dT} \geq 0 \quad \text{or} \quad \frac{dR_k(T)}{dT} \leq 0 \quad \forall k \in [1, K] \tag{6}$$

$$\frac{dC_k(T)}{dT} = 0 \quad \forall k \in [1, K]$$

A graphical illustration of the process is described in Fig. 2. The resistance of the k-th stage, calculated in case of a power dissipation P_q is defined as $R_k(T_q)$, where T_q is the temperature obtained at the input node of the given Foster network when a step with amplitude P_q is applied. For higher power dissipation values, different sets of resistive terms are obtained. Three cases of increasing power levels P_1, P_2 and P_3 are shown as an example in Fig. 2(*a*), 2(*b*) and 2(*c*), respectively. The merging of these three linear networks results in a non-linear Foster network, where each resistance non-linearity is defined as a Look-Up-Table (LUT). For instance, referring to the first stage, the LUT is defined as: $(T_1, R_1(T_1))$, $(T_2, R_1(T_2))$, $(T_3, R_1(T_3))$ which results in the network depicted in Fig. 2(*d*). It is possible to extend this procedure in order to include the effect of different ambient temperatures, resulting in a network where each resistive term is described by a double-entry LUT (Fig. 2(*e*)).

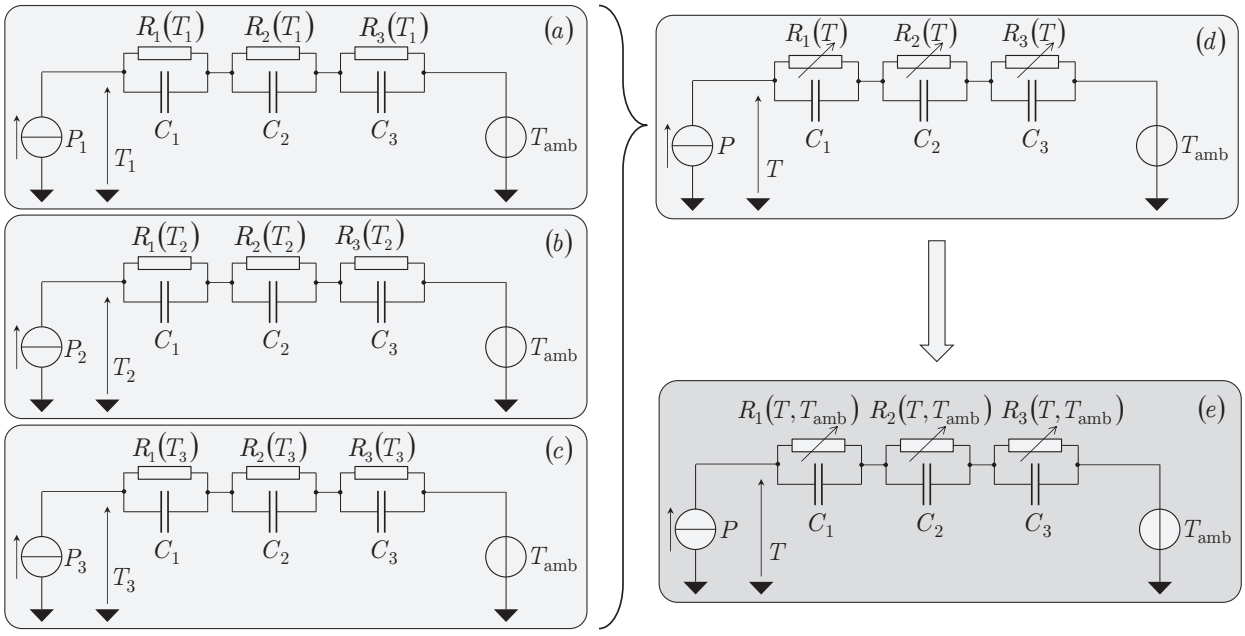

Fig. 2. Graphical illustration of the procedure to obtain non-linear Foster thermal networks. The reader should refer to the description in the text for a clarification of the process.

III. Matrix description of thermal systems

The most general representation of a system is in its MIMO (Multiple Inputs, Multiple Outputs) form. A system with N power sources and M different locations where the temperature is monitored (see for instance [26] and [27]) can be described by an $(M \times N)$ matrix definition as follows:

$$\begin{pmatrix} \Delta T_1 \\ \vdots \\ \Delta T_M \end{pmatrix} = \begin{pmatrix} Z_{11} & \dots & Z_{1N} \\ \vdots & Z_{mn} & \vdots \\ Z_{M1} & \dots & Z_{MN} \end{pmatrix} \cdot \begin{pmatrix} P_1 \\ \vdots \\ P_N \end{pmatrix} \tag{7}$$

where the indexes $m = 1, \dots, M$ and $n = 1, \dots, N$, respectively. Such description can be easily implemented in circuit simulators; an example is provided in Section V.

IV. Validation of the non-linear Foster algorithm

In this section, the algorithm to obtain non-linear Foster network is demonstrated. To do so, a non-linear FEM model of a power device was built and boundary conditions were applied in order to develop strong gradients inside the structure, and therefore, appreciable non-linearities [28], [29].

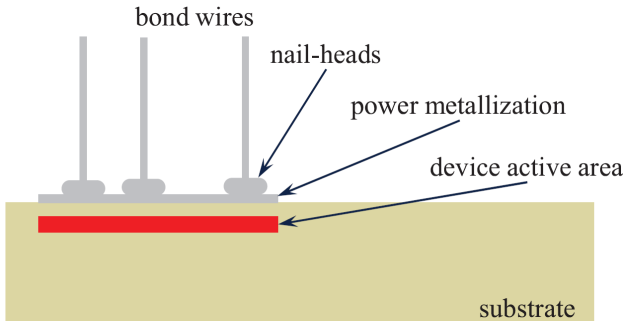

Fig. 3. Typical structure used to validate the non-linear Foster algorithm.

The bottom of such device is kept at constant temperature, while power dissipation takes place in its active area (see Fig. 3):

- for long pulses, this boundary condition is actually unrealistic, but it is numerically challenging due to the strong gradients which will take place in a transient operation, being therefore a good benchmark for the proposed algorithm;

- for short pulses, the heat wave vanishes within the thickness of the substrate, therefore the temperature at its bottom location remains almost constant; in such a case, the boundary conditions reflect a realistic condition [30], [31].

The thermal impedance of the device (corresponding to the maximum temperature) is calculated for $Q = 3$ different power dissipation levels: 10 , 220, and $440\,\mathrm{W}$. Fig. 4 shows the effect of (mainly) the substrate non-linearity on the thermal impedance for different power levels.

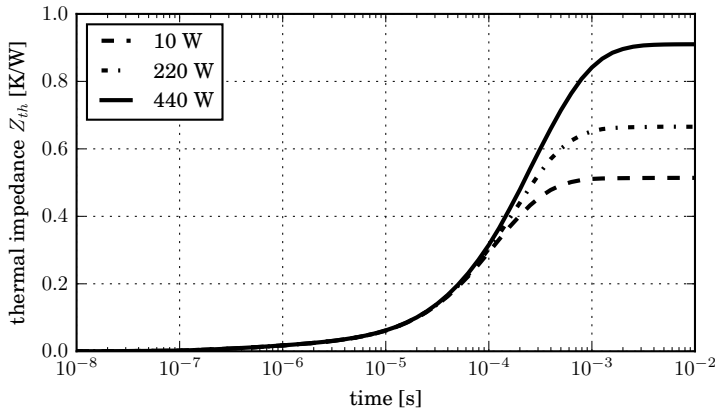

Fig. 4. Thermal impedance of the power transistor subjected to different power levels.

To better capture the non linear behavior, $Q = 45$ simulations were performed, where the power was logarithmically swept from $P_1 = 3\,\mathrm{W}$ to $P_{45} = 440\,\mathrm{W}$. A Foster network with $K = 7$ stages was found to be suitable to model such a structure.

Fig. 5 shows the *monotonic* dependence of the resistances, plotted as a function of the maximum temperature reached by the device. Obviously, the non-linear resistive terms R_k depend on the maximum temperature that was reached at every $q = 1, \ldots, Q$ power step level. Since thermal capacitance values are kept constant as a function of temperature, the time constants $\tau_i = R_i C_i$ vary in the same way as the thermal resistances.

As further validation, a series of three short-circuit pulses was chosen; the high peak power delivered during these events highlights the non-linear response of the FEM model. As it is visible in Fig. 6, the agreement between the compact and the FEM model is excellent. While such an FEM model may need up to few hours to simulate, its compact version needs few seconds. Since the determination of the model follows a methodology based on the extraction of

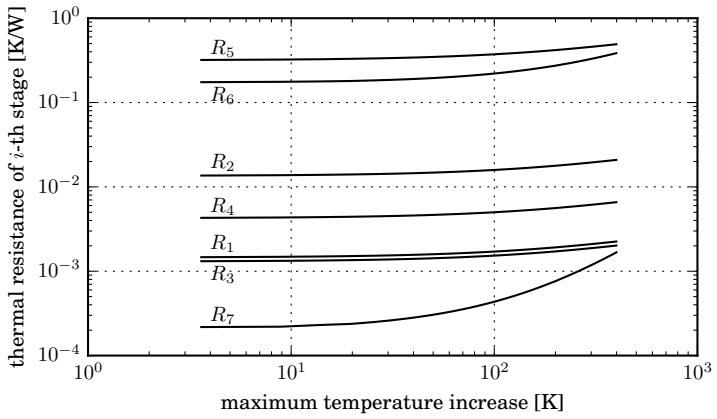

Fig. 5. Monotonic variation of the thermal resistances as a function of the maximum temperature increase in the device.

thermal impedance curves, it benefits of all the features that thermal impedance curves have, in particular, the possibility of simulating any type of pulse profile up to the steady-state domain.

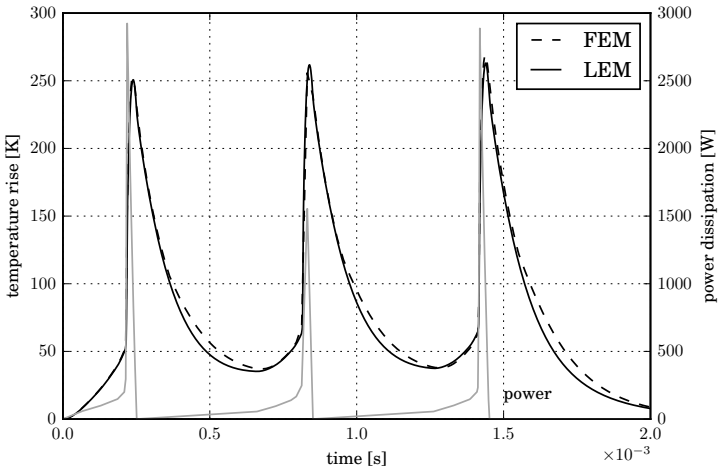

Fig. 6. Comparison between FEM model and non-linear LEM model when subjected to the shown power profile.

V. Experimental validation

In this section, the methodology is applied to a real case. An *ad-hoc* PCB was designed and manufactured, its non-linear transient thermal FEM model developed and tuned, the thermal responses of interest were extracted and the compact MIMO model developed.

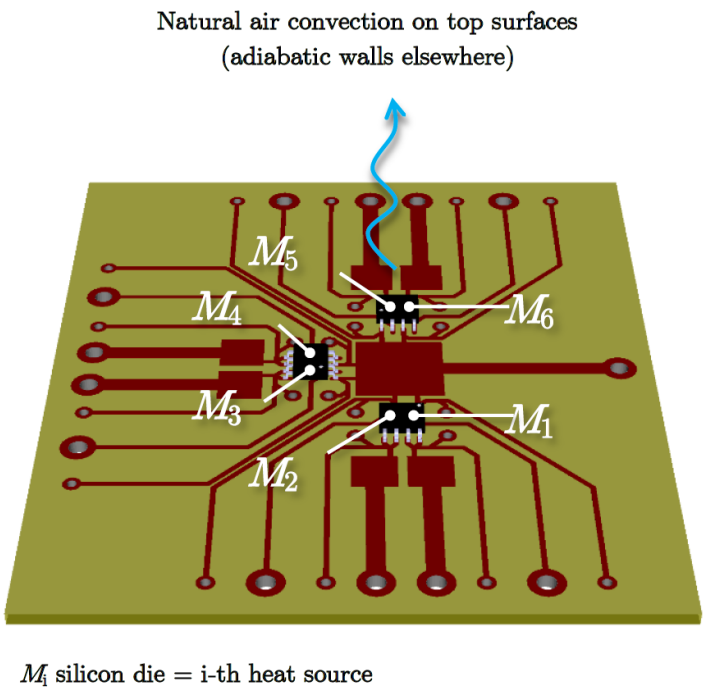

Fig. 7. Three-dimensional geometry, boundary conditions and heat sources of the fabricated PCB (designed with KiCAD 4.0.2).

A. *Test bench design and manufacturing*

The PCB is made of three MOSFETs which can be independently operated, see Fig. 7. The layout has been designed to enhance thermal interactions between components. The top side, shown in Fig. 8(*a*) was painted with an optically transparent matt paint in order to uniform emissivity on all the surfaces made of different materials. Electrical connections for biasing and test points are placed on the edges of the board, mounted on the bottom side of the PCB to keep the top side cleared of bulky components. The board is made of a $1.6\,\mathrm{mm}$ thick FR-4 substrate with $35\,\mu\mathrm{m}$ thick single copper layer. The bottom side was thermally insulated using a $6\,\mathrm{cm}$ thick layer of glass wool (Fig. 8(*b*)). The lateral surfaces of the board are small enough to neglect the heat flow across them.

Every device can be biased independently from each other (Fig. 9); temperature distribution on the overall board is recorded via IR thermography, and electrical quantities are automatically sampled via a Digital Acquisition device (DAQ).

B. *Tuning of the FEM model*

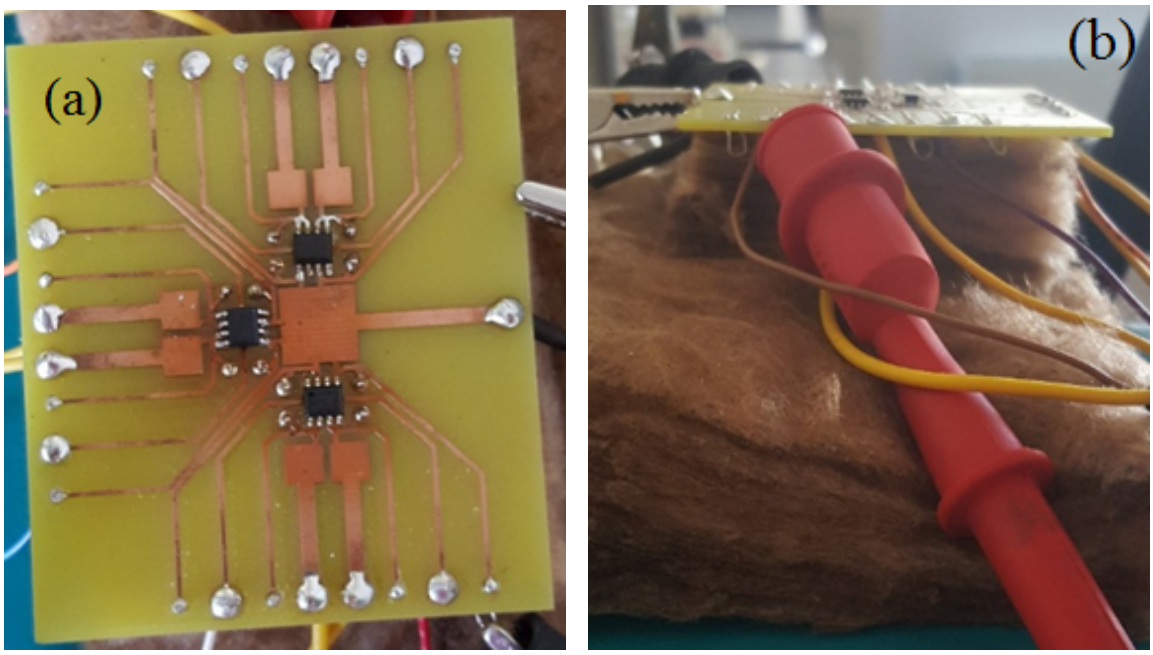

Fig. 8. The multisource test board: (a) top view; (b) side view (insulation with glass wool to assume almost perfect thermal insulation on the PCB's bottom side).

Thermal material properties are usually temperature dependent; for instance, temperature dependence of thermal conductivity of Silicon and Silicon Carbide composites can be found in [32]—[34], respectively. Usually, such kind of dependencies are already implemented in the simulation software material library.

The heat transfer coefficient h which models natural convection was instead modeled as follows (a typical non-linear function which models the fact that heat exchange efficiency increases with temperature difference between the surface and the surrounding ambient):

$$h = \alpha(T - T_{amb})^{\beta} \tag{8}$$

To judge the goodness of the fitting parameters, the following figure of merit was used:

$$|\varepsilon\%| = \frac{|\Delta T_{meas} - \Delta T_{sim}|}{\Delta T_{meas}} \cdot 100 \tag{9}$$

where ΔT_{meas} is the average measured increase over the ambient temperature, and ΔT_{sim} is the average simulated increase over ambient temperature. Maximum error of 10% was allowed. Surface-averaging was performed over *half* top surface of each device's mold compound (since

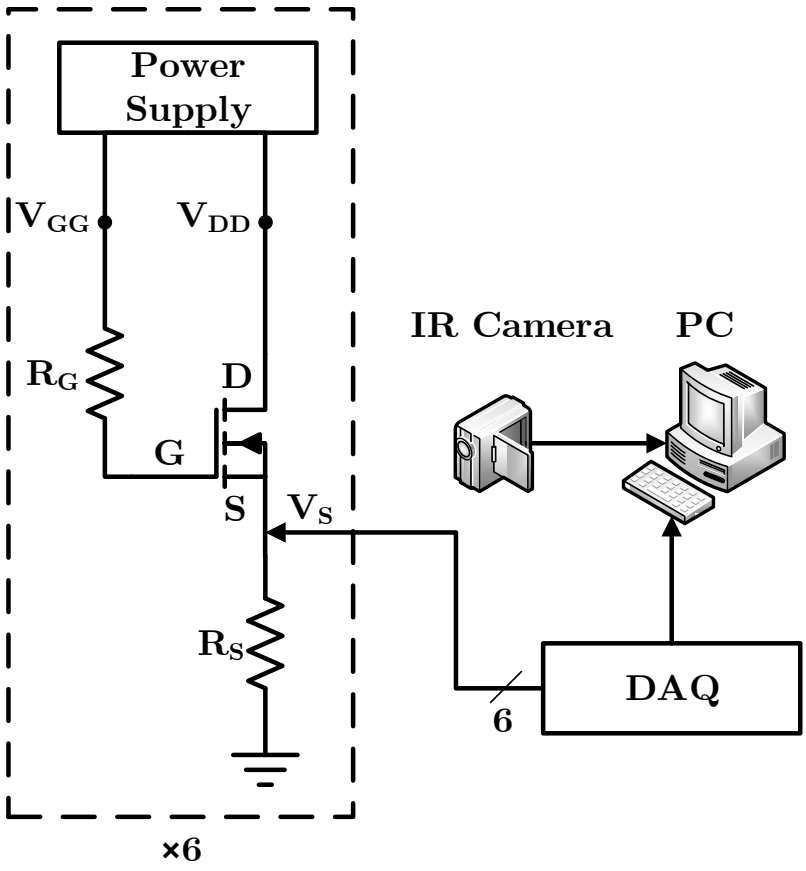

Fig. 9. Schematic diagram of the test bench built to validate the FEM modeling of a MIMO system. An infrared camera is used to measure the temperature of the surfaces exposed to the air, a Data Acquisition board (DAQ) is used to measure the voltage of the MOSFETs' source V_S, used to evaluate the voltage V_{DS} and the current I_D. All the data are collected by a PC.

every package contains to devices):

$$T_{avg} = \int_{Area/2} T(x, y)\, dA \tag{10}$$

This is usually a post-processing quantity already available in COMSOL Multiphysics. A series of measurements at different power dissipation levels allowed to find the coefficients in Equation (8) as $\alpha = 7\,\mathrm{Wm^{-2}K^{-(1+\beta)}}$ and $\beta = 0.155$. Table I and II show the errors when using such coefficients, always well below the 10% threshold. Once validated, FEM simulations are used to extract $Z_{mn}(T)$. The procedure is described in the following subsection.

TABLE I

ERRORS EVALUATION ON DEVICES TURNED ON

Device ON (dissipated power)	$\Delta T_{meas} - \Delta T_{sim}$ [K]	$\lvert\varepsilon\%\rvert$
M_1 (0.68 W)	3.4	4.7
M_2(0.64 W)	0.4	0.6
M_3(0.60 W)	−3.7	5.3
M_4(0.58 W)	−3.8	5.6
M_5(0.65 W)	−0.3	0.4
M_6(0.66 W)	2.1	2.9

TABLE II

ERRORS EVALUATION ON DEVICES BESIDE THE ONE TURNED ON

Device ON (dissipated power)	$\Delta T_{meas} - \Delta T_{sim}$ [K]	$\lvert\varepsilon\%\rvert$
M_1 (0.68 W)	2.6	5.1
M_2(0.64 W)	0.3	0.6
M_3(0.60 W)	0.6	1.3
M_4(0.58 W)	−3.2	6.4
M_5(0.65 W)	2.9	5.8
M_6(0.66 W)	2.8	5.6

C. Validation of the FEM model

The FEM model was validated against infrared thermal measurements, over different power levels and configurations. As an example, the comparison between measured and simulated temperature distribution (Fig. 10) for a particular case is shown.

Good agreement between FEM model and measurements was found. Therefore the FEM model will be used to generate the transient self- and mutual-impedances curves, to be processed by the non-linear Foster fit algorithm.

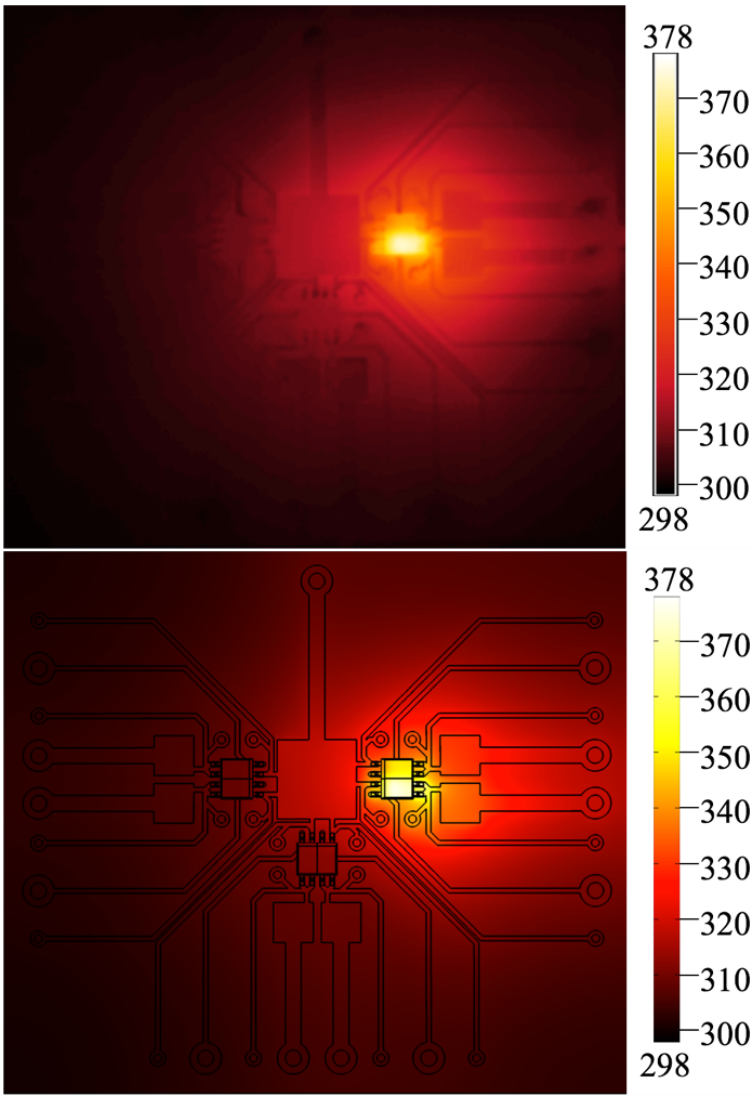

Fig. 10. Measured temperature (top) and simulated temperature (bottom) of the test board top surface with M_2 ON dissipating 640 mW, M_1, M_3, ..., M_6 OFF, and $T_{amb} = 298$ K.

D. Determination of the Z-matrix representing the system

Indexing with m the location of interest (i.e., the response location), and with n the device dissipating a certain power P, the terms of the Z-matrix are calculated as:

$$Z_{mn} = \left.\frac{\Delta T_m}{P_n}\right|_{P_l=0,\forall l\neq n}$$

$$\text{for } m = 1,\ldots,M \text{ and } n = 1,\ldots,N \quad (11)$$

TABLE III

ERRORS EVALUATION AT STEADY STATE IN THE THREE CASES CONSIDERED TO TEST THE 3-BY-3 MIMO LUMPED ELEMENT MODELLING (LEM) WITH NON-LINEAR RESISTANCES

Case study	M_2 $\lvert\varepsilon\%\rvert$	M_4 $\lvert\varepsilon\%\rvert$	M_6 $\lvert\varepsilon\%\rvert$
1	3.28	3.30	3.27
2	4.20	2.94	1.98
3	0.55	2.54	2.59

where $\Delta T_m = T_m - T_{amb}$. Considering the q-th level of the power steps, Equation (11) can be rewritten as:

$$Z_{mn,q} = \left.\frac{\Delta T_{m,q}}{P_{n,q}}\right|_{P_l=0,\forall l\neq j}$$

$$\text{for } m = 1,\ldots,M \text{ and } n = 1,\ldots,N \quad (12)$$

Once all the non-linear $Z_{mn}(T)$ are obtained, it is possible to fill the Z-matrix whose terms are non-linear Foster networks. The validated FEM model of the board depicted in Fig. 7 was used to generate a 3-by-3 MIMO description of the system, where each input is the dissipated power in the MOSFETs M_2, M_4 and M_6, and the outputs are the temperatures of the same devices T_2, T_4, and T_6:

$$\begin{pmatrix} \Delta T_2 \\ \Delta T_4 \\ \Delta T_6 \end{pmatrix} = \begin{pmatrix} Z_{22} & Z_{24} & Z_{26} \\ Z_{42} & Z_{44} & Z_{46} \\ Z_{62} & Z_{64} & Z_{66} \end{pmatrix} \cdot \begin{pmatrix} P_2 \\ P_4 \\ P_6 \end{pmatrix} \quad (13)$$

An implementation of the matrix (13) in SPICE can be shown in Fig. 11.

The Z_{mn} terms were extracted from FEM simulations with $T_{amb} = 298\,\mathrm{K}$ and $Q = 7$ different power steps with $P_q = 0.05, 0.1, 0.2, 0.3, 0.4, 0.5, 0.6\,\mathrm{W}$. Each device was turned on with the different power steps, while the others were kept off. Then, (3×7) transient simulations were ran to obtain the $(3 \times 3 \times 7)$ $Z_{mn,q}(t)$ needed to extract the non-linear Foster networks associated to the Z-matrix.

The number of simulations which are actually needed to fill *any* Z-matrix is defined by the product $(M \times Q)$, where M is the number of independent heat sources which will be actually

operating in the system (in this case, M_2, M_4 and M_6, each of which turned on singularly), and Q is the number of power dissipation levels needed to accurately capture the non-linearity in the system. The number of observed responses will not create the need of new simulations, since from the FEM simulation, every point in the structure is already available as an observable response.

Back to the system here considered, once computed the (3×7) non-linear Foster networks, the responses of the lumped element model with the ones obtained by FEM simulations in three different cases were compared:

1) Application of three equal steps at the same time to M_2, M_4, and M_6 with a power level of $0.4\,\mathrm{W}$;
2) Application of three different steps at the same time to M_2, M_4, and M_6 with power levels of 0.2, 0.35 and $0.5\,\mathrm{W}$ respectively;
3) Application of three different steps at the same time to M_2, M_4, and M_6 with power levels of 0.55, 0.15 and $0.025\,\mathrm{W}$ respectively.

In order to challenge the model, thermal situations which are different from those used to generate the model were chosen Table III shows the relative errors at steady state between FEM and SPICE simulations in these three cases. Fig. 12 shows this difference relatively to the third case.

Results are quite good and prove the validity of the proposed approach with multiple heat sources. The maximum recorded $|\varepsilon\%|$ is smaller than 5%.

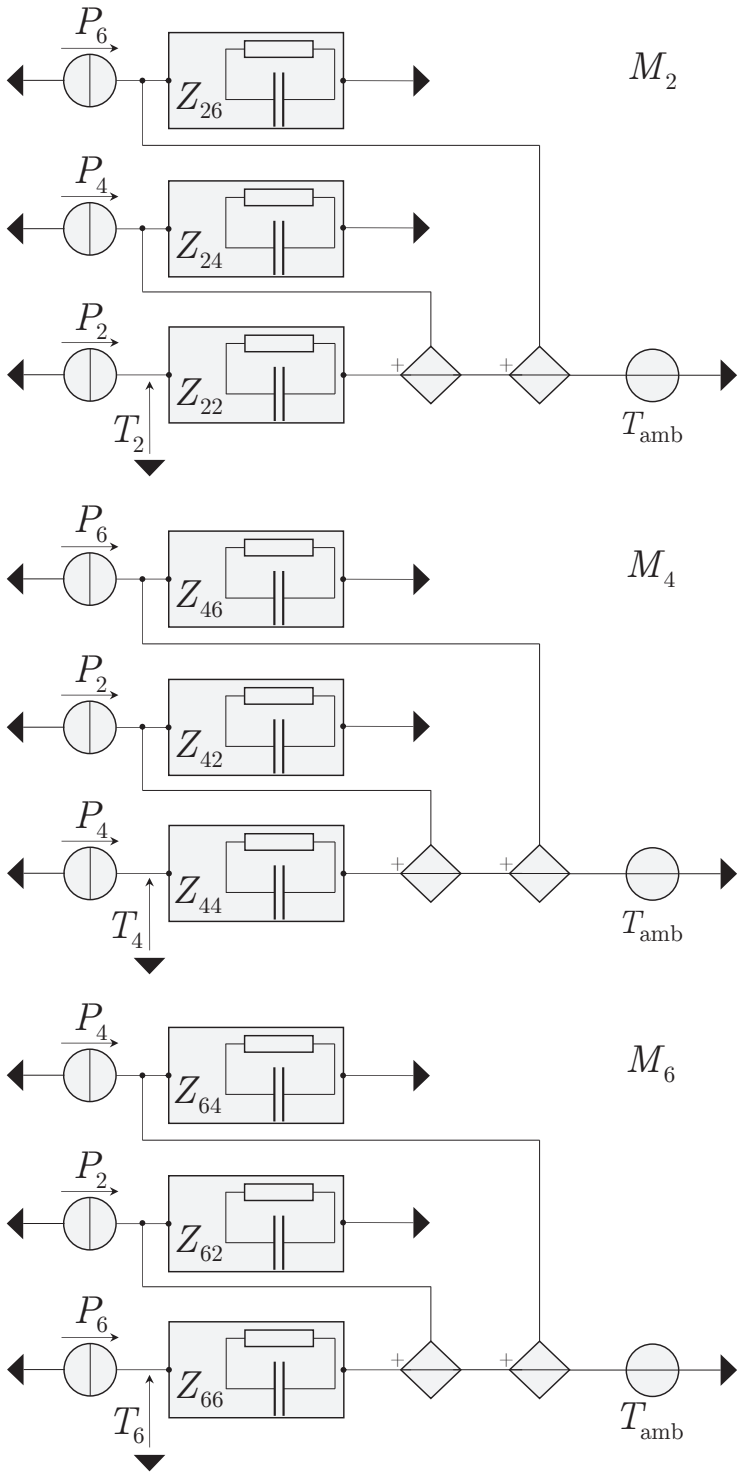

Fig. 11. Schematic of the equivalent electric circuit of a 3-by-3 MIMO system, which can be processed to extract a 3-by-3 matrix of non-linear Foster networks using the board of Fig. 7.

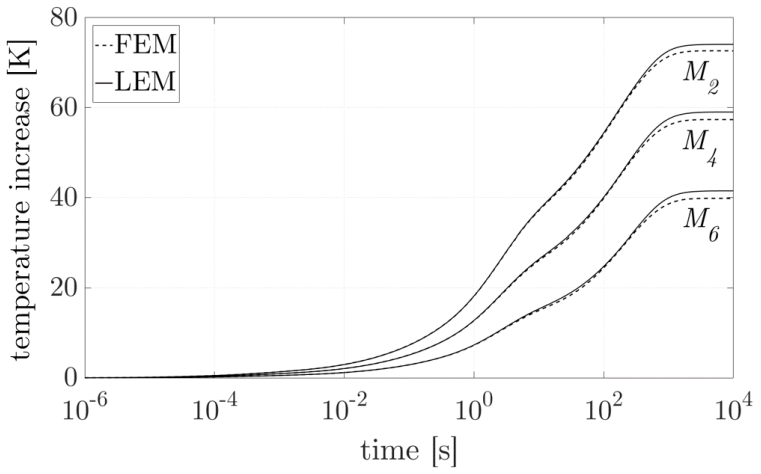

Fig. 12. $T_i - T_{amb}$ of the (3×3) MIMO system applying contemporary power steps of levels $P_2 = 550\,\mathrm{mW}$ to M_2, $P_4 = 150\,\mathrm{mW}$ to M_4 and $P_6 = 25\,\mathrm{mW}$ to M_6. T_{amb} is 298 K.

VI. Discussion and conclusions

This work proposes a robust and general way to determine non-linear Foster networks which can be suited to describe accurately the behaviour of thermal systems with strong non-linearities, multiple power dissipation nodes and multiple observed respones.

The natural and straightforward application of such models lies in its coupling with other models (e.g. electro-thermal models of electron devices) to build a fully-coupled, multi-physical simulation framework which can be solved by electrical simulators, or to simulate long and complex mission profiles, where a fast solving model is needed.

The methodology is based on a *family* of thermal impedance curves, which capture the effect of non-linearities in the system. These curves may well be obtained by a carefully tuned FEM model of the system, as showed in this work, or directly from measurements, if available. The author's suggestion is to proceed firstly by a careful development of an appropriate FEM model, from which extracting all the needed thermal impedance curves.

The validation of the approach has followed two steps. Firstly, the determination of the non-linear Foster network has been performed using a non-linear transient FEM benchmark simulation of a MOSFET under high power dissipation levels.

Modelling of MIMO systems is performed assuming that the different non-linear contributions can be linearly superposed, thus allowing a Z-matrix description which can be directly implemented in a SPICE simulator. The validity and the limitations of this assumption were evaluated on an *ad-hoc* developed PCB. Good agreement between measurements, FE model and compact model was achieved. Despite the linear superposition would theoretically not be justified, it leads anyway to small errors.

The great benefit of such models relies in the small amount of time needed for their simulations. Once computed, the lumped element model requires a lower computational effort to be simulated compared to the one needed for FEM simulations, and it can be easily integrated with electro-thermal models of electron devices, contrarily to FEM. For example, with the workstation used for this work, a transient FEM simulation can be completed in about 4 hours, while the SPICE equivalent simulation terminates in around 1 minute.

As a final remark, the algorithm to extract the non-linear Foster networks has been developed entirely in Python. The graphs have been produced by Matplotlib [35], [36]. The electrical

simulations were performed by using LT-Spice IV [37] which offers the capability to define non-linear elements (resistors, in this context) via use of LUTs and behavioral models.

VII. Acknowledgements

This work was jointly funded by the Austrian Research Promotion Agency (FFG, Project No. 846579) and the Carinthian Economic Promotion Fund (KWF, contract KWF-1521/26876/38867).

References

[1] V. Szekely, "On the representation of infinite-length distributed RC one-ports," *IEEE Transactions on Circuits and Systems*, vol. 38, no. 7, pp. 711-719, 1991.

[2] V. Szekely, "Identification of RC networks by deconvolution: chances and limits," *IEEE Transactions on Circuits and Systems I: Fundamental Theory and Applications*, vol. 45, no. 3, pp. 244-258, 1998.

[3] V. Szekely, M. Rencz, A. Poppe and B. Courtois,"New way for thermal transient testing [IC packaging]," *Semiconductor Thermal Measurement and Management Symposium*, 1999. Fifteenth Annual IEEE, San Diego, CA, USA, 1999, pp. 182-188.

[4] H. I. Rosten, C. J. M. Lasance, J. D. Parry, "The World of Thermal Characterization According to DELPHI—Part I: Background to DELPHI," *IEEE Transactions on Components, Packaging, and Manufacturing Technology*, Part A, Vol. 20, No. 4, 1997.

[5] H. I. Rosten, C. J. M. Lasance, J. D. Parry, "The World of Thermal Characterization According to DELPHI—Part II: Experimental and Numerical Methods," *IEEE Transactions on Components, Packaging, and Manufacturing Technology*, Part A, Vol. 20, No. 4, 1997.

[6] D. Schweitzer, "Thermal Transient Multisource Simulation Using Cubic Spline Interpolation of Zth Functions," *Proc. Therminic*, 2006.

[7] L. Codecasa et al., "*Circuit-based electrothermal simulation of power devices by an ultrafast nonlinear MOR approach*", IEEE Transactions on Power Electronics 31.8 (2016): 5906-5916.

[8] M. Bernardoni, N. Delmonte, G. Sozzi, R. Menozzi, "Large-signal GaN HEMT electro-thermal model with 3D dynamic description of self-heating," *Proc. IEEE Solid-State Device Research Conference* (ESSDERC), pp. 171-174, 2011.

[9] P. E. Bagnoli, C. Casarosa, M. Ciampi and E. Dallago, "Thermal resistance analysis by induced transient (TRAIT) method for power electronic devices thermal characterization. I. Fundamentals and theory," *IEEE Transactions on Power Electronics*, vol. 13, no. 6, pp. 1208-1219, 1998.

[10] P. E. Bagnoli, C. Casarosa, M. Ciampi and E. Dallago, "Thermal resistance analysis by induced transient (TRAIT) method for power electronic devices thermal characterization. II. Practice and experiments," *IEEE Transactions on Power Electronics*, vol. 13, no. 6, pp. 1220-1228, Nov 1998.

[11] P. Evans, A. Castellazzi, C. Johnson, "Automated fast extraction of compact thermal models for power electronic modules," *IEEE Trans. Power Electron.*, vol. 28, no. 10, pp. 4791-4802, Oct. 2013.

[12] Y. Gerstenmaier, A. Castellazzi, G. Wachutka, "Electrothermal simulation of multichip-modules with novel transient thermal model and time-dependent boundary conditions," *IEEE Trans. Power Electron.*, vol. 21, no. 1, pp. 45-55, Jan. 2006.

[13] A. Castellazzi, "Comprehensive compact models for the circuit simulation of multichip power modules," *IEEE Trans. Power Electron.*, vol. 25, no. 5, pp. 1251-1264, May 2010.

[14] P. R. Wilson, J. N. Ross, A. D. Brown, "Simulation of magnetic component models in electric circuits including dynamic thermal effects," *IEEE Trans. on Power Electron.*, 17(1), 55-65.

[15] A. Akturk, N. Goldsman, G. Metze, "Self-consistent modeling of heating and MOSFET performance in 3-d integrated circuits," *IEEE Trans. on Electron Devices*, 52(11), 2395-2403, 2005.

[16] M. Iachello, V. De Luca, G. Petrone, N. Testa, L. Fortuna, G. Cammarata, S. Graziani and M. Frasca, "Lumped Parameter Modeling for Thermal Characterization of High-Power Modules," *IEEE Transactions on Components, Packaging and Manufacturing Technology*, vol. 4, no.10, pp. 1613-1623, Oct. 2014.

[17] P. Cova, M. Bernardoni, N. Delmonte, R. Menozzi, "Dynamic electro-thermal modeling for power device assemblies," *Microelectronics Reliability*, 51, 9, 1948-1953, 2011.

[18] D. Chiozzi, M. Bernardoni, N. Delmonte, P. Cova, "A simple 1-D finite elements approach to model the effect of PCB in electronic assemblies," *Microelectronics Reliability*, 58, 126-132, 2016.

[19] P. Cova, N. Delmonte and R. Menozzi, "Thermal modeling of high frequency DCDC switching modules: electromagnetic and thermal simulation of magnetic components," Microel. Reliab., Vol. 48, pp. 1468-1472, 2008.

[20] M. Bernardoni, P. Cova, N. Delmonte and R. Menozzi, "Heat management for power converters in sealed enclosures: a numerical study," *Microel. Reliab.*, Vol. 49, pp. 1293-1298, 2009.

[21] Kiffe, W., and Wachutka, G. (2007). Combination of Thermal Subsystems Modelled by Rapid Circuit Transformation. *Proc. Therminic*, 2007.

[22] Online documentation at `https://www.python.org/`.

[23] Online documentation at `http://www.numpy.org/`.

[24] Online documentation at `https://www.scipy.org/`.

[25] M. Rencz and V. Szekely, "Studies on nonlinearity effects in dynamic compact model generation of packages," *IEEE Transactions on components and packaging technologies*, vol. 27, n. 1, pp. 124-130, Apr. 2004.

[26] Nenadovic, N., Mijalkovic, S., Nanver, L. K., Vandamme, L. K., d'Alessandro, V., Schellevis, H., Slotboom, J. W., "Extraction and modeling of self-heating and mutual thermal coupling impedance of bipolar transistors," *IEEE Journal of Solid-State Circuits*, 39(10), 1764-1772.

[27] K. Gorecki and M. Rogalska, "The compact thermal model of pulse transformer," *Microelectronics Journal*, vol. 45, no. 12, p. 1795-1799, Dec. 2014.

[28] K. Gorecki, J. Zarebski, "Nonlinear Compact Thermal Model of Power Semiconductor Devices," *IEEE Transactions on Components and Packaging Technologies*, vol. 33, no. 3, pp. 643-647, Sep. 2010.

[29] M. Kaminski, M. Janicki and A. Napieralski, "Application of RC equivalent networks to modeling of non-linear thermal phenomena," *Proc. 14th International Conference on Mixed Design of Integrated Circuits and Systems*, pp. 357-362, 2007.

[30] S. Eiser, M. Bernardoni, M. Nelhiebel and M. Kaltenbacher, "Finite-Element Analysis of Coupled Electro-Thermal Problems With Strong Scale Separation," *IEEE Transactions on Power Electronics*, vol. 32, no. 1, pp. 561-570, Jan. 2017.

[31] M. Nelhiebel, R. Illing, T. Detzel, S. Wöhlert, B. Auer, S. Lanzerstorfer, M. Rogalli, W. Robl, S. Decker, J. Fugger, M. Ladurner, "Effective and reliable heat management for power devices exposed to cyclic short overload pulse," *Microelectron. Rel.*, vol. 53, no. 911, pp. 1745-1749, 2013.

[32] W.M. Yim, R.J. Paff, J. Appl. Phys. 45, (1974) 1456-1457.

[33] G. G. Gadzhiev, Sh. M. Ismailov and M. M. Khamidov, *Thermal conductivity of silicon carbide ceramics doped with beryllium oxide*, Journal of Inorganic Materials, vol. 36, no. 2, pp. 197-199, 2000.

[34] W. Janke, A. Hapka, "Nonlinear thermal characteristics of silicon carbide devices," *Material Science and Engineering: B*, vol. 176, no. 4, pp. 289-292, Mar. 2011.

[35] Online documentation at `http://matplotlib.org/`.

[36] J. D. Hunter, "Matplotlib: A 2D graphics environment," *IEEE Computing In Science & Engineering*, vol. 9, no. 3, pp. 90-95, 2007.

[37] Online documentation at `http://www.linear.com/designtools/software/`.